BIOCHEMISTRY
including biophysical chemistry & molecular biology

Article

pubs.acs.org/biochemistry

Halide and Proton Binding Kinetics of Yellow Fluorescent Protein Variants

Harriet E. Seward, Jaswir Basran, Roanne Denton, Mark Pfuhl,† Frederick W. Muskett, and Clive R. Bagshaw*

Department of Biochemistry, University of Leicester, Leicester LE1 9HN, U.K.

Supporting Information

ABSTRACT: A T203Y substitution in green fluorescent protein causes a red shift in emission to yield a class of mutants known as yellow fluorescent protein (YFP). Many of these YFP mutants bind halides with affinities in the millimolar range, which often results in the chromophore p*K* values being shifted into the physiological range. While such sensitivities may be exploited for halide and pH sensors, it is desirable to reduce such environmental sensitivities in other studies, such as in Förster resonance energy transfer probes to measure conformational changes within fusion proteins. Venus and Citrine are two such variants that have been developed with much reduced halide sensitivities. Here we compare the kinetics of halide binding, and the coupled protonation reaction, for several YFP variants and detect slow kinetics (dissociation rate constants in the range of 0.1−1 s^{-1}), indicative of binding to an internal site, in all cases. The effective halide affinity for Venus and Citrine is much reduced compared with that of the original YFP 10C construct, primarily through a reduced association rate constant. Nuclear magnetic resonance studies of YFP 10C confirm halide binding occurs on a slow time scale (<4 s^{-1}) and that perturbations in the chemical shift occur throughout the sequence and structure.

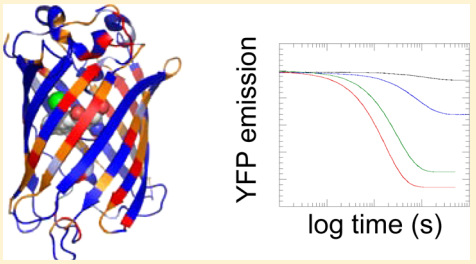

The fluorescence emission spectra of GFP and its derived variants are pH-dependent, a property that requires a full understanding for the application of these proteins as probes in vitro, as well as in living cells. The ratio of the highly fluorescent anionic state of the chromophore (the so-called B-state) to the protonated state (the so-called A-state) depends on the local environment of the chromophore, its connectivity to proton acceptors within the protein, and the external pH.[1,2] The fluorescent anionic chromophore of wild-type GFP makes a relatively minor contribution at neutral pH, a characteristic that was overcome by the S65T mutation in the widely used enhanced eGFP variant.[1] Nevertheless, eGFP has a p*K* of ∼6.0, so that the protonated state still makes a small but significant contribution at physiological pH values. Furthermore, some YFP variants have p*K* values approaching or exceeding 7, particularly in the presence of chloride or other halides,[3] so that the weakly fluorescent protonated chromophore may dominate under physiological conditions. YFP variants showing reduced sensitivity to pH and halides have been developed (e.g., Citrine[4] and Venus[5,6]), particularly for as use as Förster resonance energy transfer (FRET) probes where an environment-independent emission of the donor and acceptor is critical.[7] Nevertheless, these proteins may still bind halides under some conditions.[8] On the other hand, mutations such as H148Q enhance halide binding and have been incorporated to make halide sensors.[9−11]

Previous studies have shown there is a tight coupling between protonation and halide binding in YFP variants.[9,12,13] X-ray crystallography has revealed that a halide binding site is positioned close to the chromophore and stabilized, in part, by tyrosine 203, which is the characteristic mutation (T203Y) of many YFP variants.[12,13] In addition, surface-bound halides were identified away from the chromophore. The exact position of the bound halide relative to the chromophore is different in YFP-H148Q [Protein Data Bank (PDB) entry 1f09[12]] and E^2GFP (PDB entry 2o24[13]), but both are close (4.2−4.5 Å) to the chromophore heterocyclic carbonyl oxygen that carries a negative charge in one tautomeric form. The negative charge of the halide is thought to suppress the ionization of the chromophore and hence increase the p*K* of the latter. Understanding the coupling between halide and proton binding is important in designing halide and pH sensors.[14] It is also important to elucidate the kinetics of these interactions so that the fluorescence time courses probed by YFP and its variants can be fully interpreted. For example, guanidinium hydrochloride has been employed as a denaturant to study YFP unfolding, but at the concentrations used, chloride ion binding may well precede unfolding and hence contribute to the fluorescence time course.[8,15]

Previously, we investigated the kinetics of protonation of the commercially available YFP 10C variant and found slow kinetics (rate constants of ∼1 s^{-1}) on jumping the pH with chloride-containing buffers.[16] We extend these studies to other variants and determine the influence of halides on the kinetics.

Received: December 20, 2012
Revised: February 27, 2013
Published: March 20, 2013

dx.doi.org/10.1021/bi3016839 | *Biochemistry* 2013, 52, 2482−2491

These measurements extend published investigations conducted at equilibrium and offer insight into the coupling between halide and proton binding. We have also conducted nuclear magnetic resonance (NMR) measurements on the mYFP 10C variant to probe the effect of halide on the conformational dynamics of the protein.

MATERIALS AND METHODS

YFP Cloning and Preparation. The YFP 10C clone was obtained from Clontech (BD Biosciences, Oxford, U.K.), and the sYFP clone was a gift from D. Gadella. Mutations were introduced using the Stratagene QuikChange mutagenesis kit to construct other variants (Table 1). Proteins were expressed with an N-terminal His tag in *Escherichia coli* strain BL21 using a pET28a+ expression vector and purified as described previously.[16] For NMR spectroscopy, isotopically labeled mYFP 10C was produced by expression in BL21(DE3) pLys S cells cultured in M9 minimal medium containing $^{15}NH_4Cl$ and uniformly ^{13}C-enriched glucose for doubly labeled samples. Preparations were dialyzed extensively in 20 mM sodium phosphate buffer (pH 7) to remove halide ions from the stock proteins.

Table 1. Amino Acid Substitutions in YFP Variants[a]

YFP variant	substitutions vs wild-type GFP	ref
E^2GFP	F64L, S65T, T203Y	25
YFP 10C	S65G, V68L, S72A, T203Y	1
Citrine	S65G, V68L, Q69M, S72A, T203Y	4
sYFP	F46L, F64L, S65G, S72A, M153T, V163A, S175G, T203Y	24
Venus	F46L, F64L, S65G, V68L, S72A, M153T, V163A, S175G, T203Y	5

[a]In addition, the monomeric variants used here contain an A206K substitution.

Spectrophotometric Measurements. Equilibrium absorbance and fluorescence measurements were taken in a Cary 50 spectrophotometer (Varian Ltd., Walton-on-Thames, U.K.) and an SLM 8000 fluorometer, respectively. Stopped-flow measurements were performed using a SX18MV instrument (Applied Photophysics Ltd., Leatherhead, U.K.) using an excitation wavelength of 514 nm and a 530 nm cutoff emission filter as described previously.[16] Reactions were assessed in a 20 mM sodium phosphate buffer (pH 5.5−8), supplemented with sodium halides or other anions as indicated, at 20 °C. The pH values of all solutions were checked after the final reaction buffer had been created. All concentrations refer to those in the reaction chamber after mixing. Reactions were assessed on a logarithmic time base and analyzed by fitting to a single-exponential function using Kaleidagraph (Synergy Software, Reading, PA). Estimates of fitted rate constants generally returned standard errors of <1 and <2% for the smallest amplitudes that were analyzed. Usually, three records were obtained for each condition, and the fitted parameters (k_{obs}, amplitude, and baseline) for each agreed within <10%.

NMR Spectroscopy. ^{15}N HSQC spectra were recorded using a sample of 0.6 mM mYFP 10C in a buffer composed of 20 mM sodium phosphate (pH 7.0) and 0.02% NaN_3 at 303 K and a ^1H resonance frequency of 800 MHz (Bruker Avance spectrometer). To probe the effect of F^- ions, spectra were recorded with and without the addition of 10 mM NaF. For assignments, combined $^1H-^{15}N$ chemical shift perturbations were calculated via CCPN analysis using the standard weighting of 0.2 for ^{15}N. Exchanging peak pairs were identified using the minimal chemical shift method[17,18] combined with consideration of neighboring peaks to obtain the most likely identification of new peaks.

RESULTS

YFP 10C. Previously, we reported that when the pH of a solution containing YFP 10C in a buffer containing 40 mM NaCl was changed, there was a slow phase (k_{obs} of ~1 s^{-1}) in the fluorescence change that we interpreted as a proton-coupled conformational change.[16] Subsequently, we found YFP 10C undergoes dimerization at low pH[19] and therefore questioned whether the slow phase in fluorescence might arise from changes in the dimerization state. We therefore re-examined the kinetics using the YFP 10C A206K mutant construct[20] to promote the monomeric state and found the kinetics were identical (see Figure S1 of the Supporting Information). Hence, dimerization is not a complicating factor in these measurements. However, we have used the YFP 10C A206K variant in all the studies reported here as a precaution. More importantly, re-evaluation of the kinetics showed that the slow phase was dependent on the presence of chloride and that our original scheme (Scheme S1 of the Supporting Information) required modification to include Cl^- binding in the slow step, as in Scheme 1.

Scheme 1

$$YFP^- + H^+ \underset{k_{-1}}{\overset{k_1}{\rightleftharpoons}} YFPH + Cl^- \underset{k_{-h}}{\overset{k_h}{\rightleftharpoons}} YFPH.Cl^-$$

We consider the level of binding of Cl^- to the unprotonated YFP^- state to be negligible (see Discussion). In Scheme 1, the first step is rapid ($k_{-1} > 10^5$ s^{-1}) as determined by pressure-jump measurements[16] and in line with flash photolysis studies of other variants[21,22] and therefore not resolved by stopped-flow methods (dead time of 1.5 ms[23]). The isomerization in the absence of halide, defined by step 1b in Scheme S1 of the Supporting Information, was omitted from Scheme 1 because its contribution is minor (see the Supporting Information). In Scheme 1, the rate constant k_{obs} of the transition resolved by a stopped-flow method and induced by a rapid change in pH or Cl^- concentration is given by the relationship $k_{obs} = [H^+]/([H^+] + K_1)k_h[Cl^-] + k_{-h}$, where $K_1 = 10^{-5}$ M and $[H^+]$ refers to the pH after mixing (see the Supporting Information for the derivation). In effect, a pH increase is like a relaxation experiment in which the system adjusts to a new equilibrium position. In our previous work,[16] we estimated the forward and reverse first-order rate constants of the slow step to be ~26 and ~1 s^{-1}, respectively (k_{1b} and k_{-1b}, Scheme S1 of the Supporting Information), in 0.04 M NaCl. We now assign the forward rate constant to Cl^- binding and accordingly the second-order association constant $k_h \approx 26/0.04 = 650$ M^{-1} s^{-1}, while the dissociation rate constant for Cl^- (k_{-h}) equals 1 s^{-1}, which gives a K_h value of 1.5 mM. These constants, in conjunction with a pK_1 of 5 for the first step, yield an apparent overall relationship of $pK = pK_1 + \log[(K_h + [Cl^-])/K_h] = 6.4$ in 40 mM NaCl and an apparent K_d for binding of Cl^- to YFP at pH 7 equal to $K_h(1 + K_1/[H^+])$ (=150 mM), comparable to the results of previous equilibrium studies.[12]

dx.doi.org/10.1021/bi3016839 | *Biochemistry* 2013, 52, 2482−2491

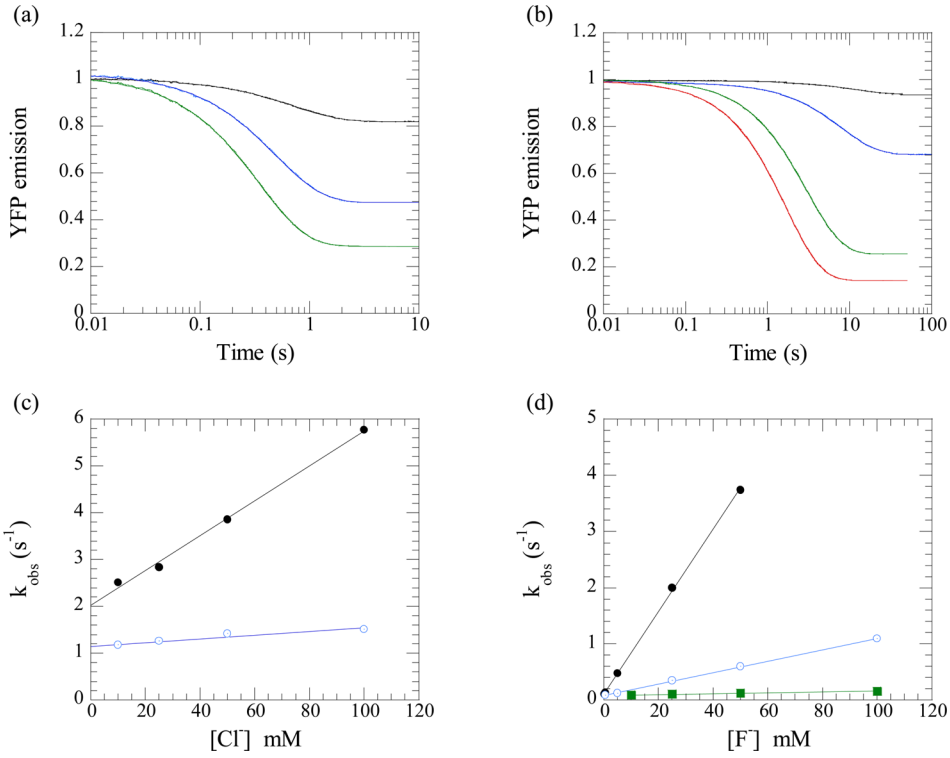

Figure 1. Chloride and fluoride ion binding to mYFP 10C. Representative stopped-flow records on mixing (a) 2.8 μM mYFP 10C with 50 (black), 250 (blue), and 500 mM NaCl (green) in 10 mM sodium phosphate buffer (pH 6.9) and (b) 2.5 μM mYFP 10C with 0.5 (black), 5 (blue), 25 (green), and 50 mM NaF (red) in 10 mM sodium phosphate buffer (pH 6.9). (c) Plot of the observed rate constant for Cl^- binding as a function of Cl^- concentration and pH. (d) Plot of the observed rate constant for F^- binding as a function of F^- concentration and pH at pH 6.0 (●), 6.9 (○), and 8.0 (■). All concentrations are final reaction chamber concentrations.

Table 2. Summary of the Kinetics of Binding of Cl^- and F^- to YFP Variants According to Scheme 1

		chloride					fluoride				
protein	pK	k_h[a] (M^{-1} s^{-1})	k_{-h}[b] (s^{-1})	K_h[c] (mM)	K_{app}[d] (M)	K_{rel}[e] (pH 7)	k_h[a] (M^{-1} s^{-1})	k_{-h}[b] (s^{-1})	K_h[c] (mM)	K_{app}[d] (M)	K_{rel}[e] (pH 7)
mYFP10C	5.0[f]	310	1.1	3.5	0.36	1	770	0.083	0.11	0.012	1
E^2GFP	6.6[g]	23	0.12	5.2	0.018	0.051	not determined				
sYFP	6.0[h]	1	0.08	80	0.88	2.4	18	0.14	7.8	0.086	7.2
mVenus	5.7[i]	0.32	0.08	250	5.2	15	20	0.33	17	0.35	28
mCitrine	5.5[j]	7	1.7	240	7.5	21	0.43	0.036	84	2.6	217

[a]Rate constant for binding of a halide to the protonated YFP·croH species, determined from the observed concentration dependence of binding (or K_{app}) at pH 6.9 and the stated pK value. [b]Rate constant for dissociation of a halide from the YFP·croH·halide species determined from the k_{obs} intercept value or k_{obs} at low fractional saturation. [c]$K_h = k_{-h}/k_h$. [d]Apparent equilibrium dissociation constant for binding of a halide to YFP at pH 7 determined from K_h and pK; i.e., $K_{app} = K_h(1 + 10^{pH-pK})$. Uncertainties in the p$K$ largely cancel out as the raw data were obtained at pH 6.9. [e]Relative equilibrium dissociation constant at pH 7 compared with that of YFP 10C. [f]pK from ref 16. [g]pK from ref 22. [h]pK from ref 24. [i]Effective pK in the presence of 150 mM gluconate. [j]Measured experimentally in the presence of 100 mM gluconate. All pK values refer to estimates in the absence of halide (i.e., pK_1 of Scheme 1).

Scheme 1 may be characterized by increasing the pH at a fixed halide concentration (as described above) or by increasing the halide concentration at a fixed pH. Figure 1 shows experimental records for increases in Cl^- and F^- concentrations with YFP A206K and the resultant plots of the observed rate constant, k_{obs}, as a function of halide concentration. The intercept and slopes provide estimates of k_{-h} and $k_h[[H^+]/([H^+] + K_1)]$, respectively. For F^-, $k_{-h} = 0.083$ s^{-1}, while taking a K_1 of 10^{-5} M yields a k_h value of 770 M^{-1} s^{-1} and hence a K_h of 0.11 mM. At pH 7.0, the apparent K_d for binding of F^- to YFP 10C is calculated to be 12 mM. For Cl^-, these parameters are less well-defined because the k_{obs} shows a greater dependence on pH than predicted by the equation derived for Scheme 1. Thus, k_{-h} = 1.1–2 s^{-1}, while the estimated k_h = 310–400 M^{-1} s^{-1}; hence, K_h = 3.5–5 mM, with the smaller values referring to pH 7 in each case. These values are summarized in Table 2. The derived K_h values for binding of F^- and Cl^- to the YFPH state of YPF 10C are comparable to the equilibrium titration values of Wachter et al.[12] of 0.214 and 4.69 mM, respectively. The tighter binding of F^- compared with that of Cl^- is largely due to a reduced dissociation rate constant.

Venus. Venus was developed as a yellow FRET acceptor protein by Nagai et al.[5] through selection for fluorescence brightness and rapid maturation. It was also reported to have low affinity for Cl^- (K_{app} > 10 M at pH 7.0) and a low pK (6.0) that was affected little by the presence of Cl^-, at least when the ionic strength was maintained with potassium gluconate. However, the reported pK values for Venus vary from 5.6[24]

dx.doi.org/10.1021/bi3016839 | Biochemistry 2013, 52, 2482–2491

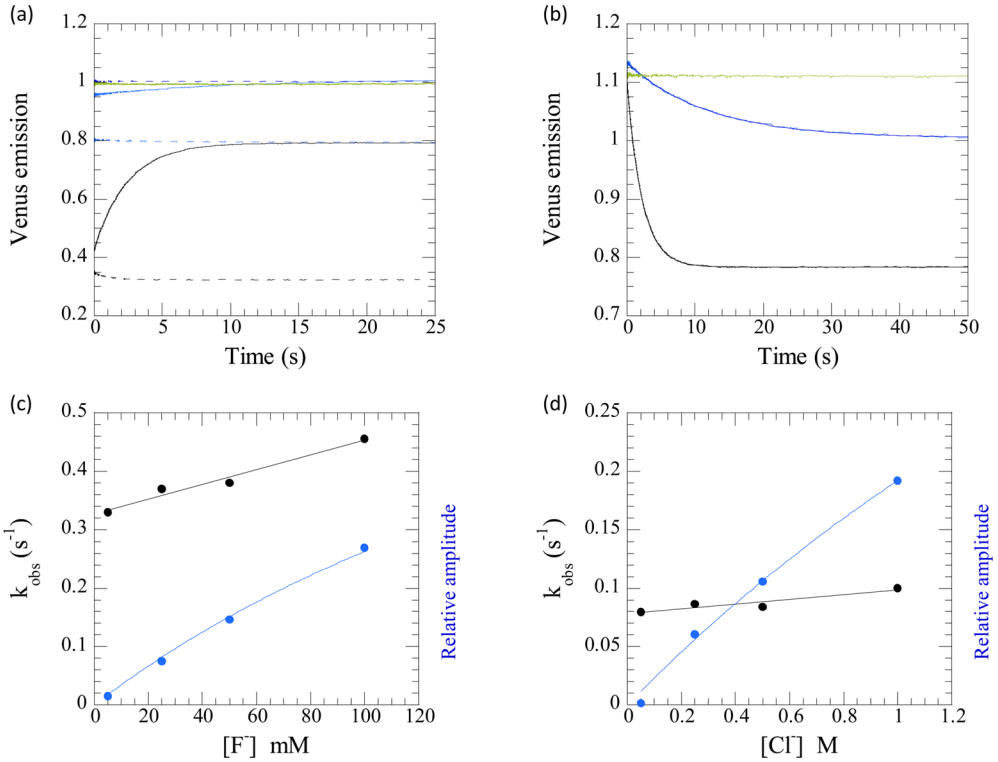

Figure 2. Halide binding to mVenus. (a) Fluorescence stopped-flow records for pH increases of 2.4 μM mVenus in 20 mM potassium phosphate buffer. Baselines (dashed lines) were established for mVenus at pH 6.0 in the presence of 50 mM Cl^- (blue dashed line at 0.8 emission) and 50 mM F^- (black dashed line at 0.35 emission) and pH 8.0 in the presence of 50 mM Cl^- (black dashed line at 1.0 emission). At pH 8.0 in the presence of 50 mM sodium gluconate, the emission signal was also at 1.0, while in the presence of 50 mM F^-, it was at 0.96 (traces omitted for the sake of clarity). pH increases were recorded for mVenus initially at pH 6.0 and then at pH 6.9 by the addition of pH 8.0 buffer in the presence of 50 mM Cl^- (blue solid line; k_{obs} = 0.086 s^{-1}), 50 mM F^- (black solid line; k_{obs} = 0.42 s^{-1}), or 50 mM gluconate (green solid line; no observed transient). The anions were present in both syringes. (b) Stopped-flow records of mVenus subject to anion concentration increases at pH 6.9. mVenus in 20 mM potassium phosphate buffer and 0.5 M sodium gluconate was mixed with an equal volume of 20 mM phosphate buffer as a control (green record) or buffer with 0.5 M NaCl (blue line; k_{obs} = 0.084 s^{-1}). mVenus in phosphate buffer was mixed with 100 mM F^- (black line; k_{obs} = 0.46 s^{-1}). (c) Dependence of k_{obs} on F^- concentration for mVenus at pH 6.9 (black line). The linear fit yielded a slope of 0.0013 mM^{-1} s^{-1} and an intercept of 0.33 s^{-1}, i.e., apparent K_d at pH 6.9 of 0.25 M. A plot of the amplitude of the signal change, relative to the total fluorescence, when forced to fit to a hyperbola (blue line) yielded an apparent K_d of 0.28 M, consistent with the rate data. (d) Dependence of k_{obs} on Cl^- concentration for mVenus at pH 6.9 (black line). The linear fit yielded a slope of 0.02 M^{-1} s^{-1} (but with a 25% error) and an intercept of 0.08 s^{-1}, i.e., apparent K_d at pH 6.9 of ≈4 M. A plot of the amplitude of the signal change, relative to the total fluorescence, when forced to fit to a hyperbola (blue line) yielded an apparent K_d of 4.2 M, confirming the rate data.

to 7.0.[8] In view of this discrepancy, we repeated the pK determination for mVenus and found it was 6.0 at low ionic strengths, but the chromophore absorbance did not approach zero at pH 5, suggesting there was a second ionization with a lower pK (Figure S2 of the Supporting Information). In the presence of 150 mM gluconate, this second pK was increased so that the two steps were not clearly resolved. Over the accessible titration range (pH 5.5−8) in the presence of 150 mM gluconate, the system behaved effectively as a single ionization with a pK of ≈5.7 (see the Supporting Information). We therefore interpreted the effect of halides on mVenus using Scheme 1 and a K_1 of $10^{-5.7}$ M.

While careful comparisons between the effects of Cl^- compared with gluconate may reveal the contribution of a specific halide effect in equilibrium titrations, we reasoned that any internally bound Cl^- would have slow kinetics (time scale of seconds), as observed for YFP 10C, and that stopped-flow measurements may provide better discrimination between the effects of gluconate and halides. We refer to these internal binding sites as being specific relative to the surface residues, although it is known they can bind a range of small anions.[9,12] We investigated binding of a halide to mVenus by pH increases in the presence and absence of halide (Figure 2a). When the pH was increased from 6 to 6.9 in the presence of 50 mM Cl^-, a low-amplitude transient was observed with a rate constant of ∼0.09 s^{-1} (Figure 2a, blue trace), although comparison with the pH 6.0 calibration signal (Figure 2a, blue dashed line) indicates most of the change occurred within the dead time of the stopped-flow instrument. In the absence of Cl^- or in presence of 50 mM sodium gluconate (Figure 2a, green trace), no transient phase was resolved, indicating that the small transient seen with Cl^- did represent a low degree of specific binding. In the presence of 50 mM F^-, the initial fluorescence of mVenus at pH 6.0 was much lower compared with that upon addition of Cl^-, and a large transient was observed (k_{obs} = 0.4 s^{-1}) when the pH was increased to 6.9 (Figure 2a, black trace). These data indicate mVenus retains a significant specific affinity for F^-.

Halide concentration increases at a constant pH (6.9) revealed the same trend and similar observed rate constants (Figure 2b) as pH increases at a fixed halide concentration (Figure 2a). The observed rate constant for F^- concentration increases in the range of 5−100 mM showed a shallow concentration dependence and an intercept of 0.33 s^{-1}; i.e., k_{obs} is dominated by the dissociation constant (k_{-h}) for dissociation

dx.doi.org/10.1021/bi3016839 | Biochemistry 2013, 52, 2482−2491

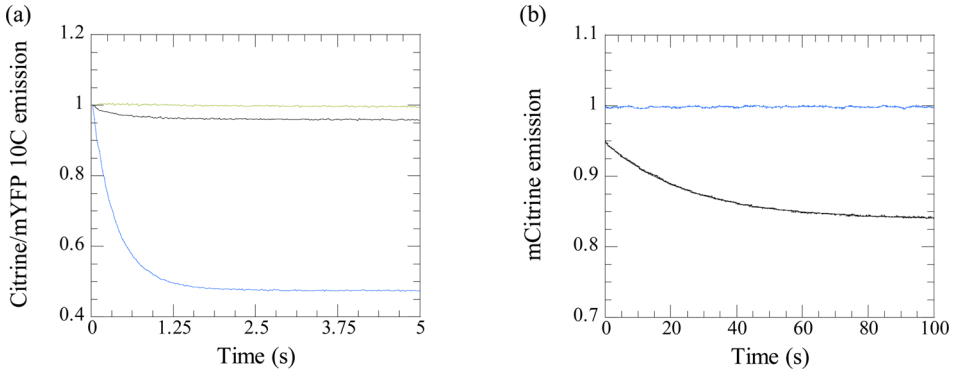

Figure 3. Halide binding to mCitrine. (a) Cl^- jump stopped-flow records for mCitrine compared with those of mYFP 10C. mCitrine (2.25 μM) was mixed with 50 mM NaCl (black line; k_{obs} = 1.8 s^{-1}) or 75 mM sodium gluconate (green line) in 20 mM potassium phosphate buffer (pH 6.2) compared with 2.25 μM mYFP 10C (blue line; k_{obs} = 2.7 s^{-1}) mixed with 50 mM NaCl. The latter trace was normalized to the same observed start level fluorescence to show the relative amplitudes of the effect of Cl^-. (b) mCitrine (3 μM) in 20 mM potassium phosphate buffer (pH 6.9) was mixed with the same buffer (blue trace) or 237 mM F^- (black trace; k_{obs} = 0.039 s^{-1}). The excitation wavelength was 515 nm, and the emission was monitored at >530 nm. All concentrations refer to the reaction chamber, and the temperature was 20 °C throughout.

of F^- from protonated mVenus (Figure 2c). The observed slope (1.3 M^{-1} s^{-1}) when combined with a macroscopic pK of 5.7 for the chromophore protonation yielded a k_h value of 20 M^{-1} s^{-1}, and thus a K_h for specific binding of F^- to protonated mVenus of 0.016 M. The amplitudes of the transients increased almost linearly with F^- (in line with k_{-h} dominating k_{obs}) but when forced to fit to a hyperbola gave an apparent K_h of 0.28 M at pH 6.9 and hence a K_h of 0.017 M, which is consistent with the rate analysis. Although there is little curvature in the amplitude plot, the maximal fluorescence change was well-defined (assuming the end point fluorescence approaches zero at a saturating F^- concentration), and hence, the apparent K_h was derived from a one-parameter fit with reasonable precision (standard error of 2.5%). In the presence of Cl^-, the amplitudes of the resolved fluorescence quench were smaller, and the slope in k_{obs} was close to zero (Figure 2d). However, the intercept defined the value of k_{-h} (0.078 s^{-1}) with good precision (±0.003 s^{-1}). When the amplitude of the process versus Cl^- concentration was forced to fit to a hyperbola, the apparent K_d for Cl^- at pH 6.9 was 4.2 M, which is close to the lower limit determined by Nagai et al.[5] This value indicates the K_h for binding of Cl^- to the protonated mVenus state was 0.25 M, and hence, k_h ≈ 0.32 M^{-1} s^{-1} (Figure 2d).

sYFP. Kremers et al.[24] found that the V68L mutation of Venus slowed the maturation of the fluorescent protein ~2-fold in bacterial systems. They therefore explored the properties of a "revertant" variant, termed sYFP, without this mutation (s for "super"; which also contained the A206K substitution to favor the monomeric form) and found it was similar to Venus in absorbance and quantum yield but had a slightly higher pK (6 cf. 5.6) in their 50 mM citrate-phosphate-glycine buffer. Binding of a halide to sYFP was explored using pH increases in the presence of 50 mM Cl^- or F^- (Figure S3a,b of the Supporting Information). The transients were similar to those of mVenus, but the amplitudes were noticeably larger. No transients were seen in the presence of 50 mM gluconate, confirming that the stopped-flow assay resolves halide-specific binding. On the basis of the relative amplitude of the resolved transient with an increase in pH from 6.0 to 6.9 in the presence of 50 mM Cl^- (amplitude of 0.17), K_h ≈ 80 mM, while in the presence of 50 mM F^- (amplitude of 0.3), K_h ≈ 8 mM. More extensive measurements were taken in the presence of F^-. Increases in fluoride concentration at a fixed pH of 6.9 confirmed that the response of sYFP was intermediate between that of mYFP10C and mVenus (Figure S3c of the Supporting Information). From the slope (0.002 mM^{-1} s^{-1}) and the intercept of the (0.14 s^{-1}) of dependency of k_{obs} on F^- at pH 6.9 (i.e., apparent K_d = 0.07 M), the value of K_h for binding of F^- to the protonated sYFP state was 7.8 mM (Figure S3d of the Supporting Information).

Citrine. Citrine was among the first YFP proteins to be developed with a reduced sensitivity to halide binding that retain favorable folding characteristics.[4] This aspect was rationalized in terms of the Q69M mutation filling the cavity occupied by halide in the eYFP H148G variant.[4,12] The observed pK of 5.7 was unaffected by the presence of 147 mM Cl^-, from which it was concluded that the effect of halide "had been eliminated" compared with that of YFP 10C.[4] As with Venus, it was necessary to control for "nonspecific" ionic strength effects using a larger anion such as gluconate that was not expected to bind in the halide cavity of YFP. We obtained a pK of 5.54 in the presence of 100 mM Cl^- and confirmed that gluconate gave a shift in pK similar to that found in studies at low ionic strengths (pK = 5.17 in 20 mM potassium phosphate buffer). To obtain a more stringent assessment of specific versus nonspecific effects, stopped-flow measurements were performed. At pH 6.9, the pH we used to study other YFP variants, the effect of 50 mM Cl^- was barely detectable. An increase in Cl^- concentration at pH 6.2 produced a much smaller transient with mCitrine (3.6% quench) than with mYFP 10C (52%), but the rate constants (1.8 s^{-1} for mCitrine and 2.7 s^{-1} for mYFP 10C) were of similar magnitude (Figure 3a), indicating that k_{obs} is dominated by k_{-h} in the case of mCitrine. On the other hand, mixing mCitrine with gluconate produced no significant transient, indicating that the quench observed in equilibrium measurements occurs within the dead time of the instrument. An amplitude of 3.6% suggests an apparent K_d for Cl^- of 1.4 M at pH 6.2 and hence a K_h of 0.24 M for the protonated state. An increase to 237 mM F^- at pH 6.9 produced an 11% resolved quench in fluorescence, indicating an apparent K_d of 2.1 M and hence a K_h of 84 mM for the protonated state (Figure 3b). These measurements confirm that mCitrine binds halide ions much more weakly than mYFP 10C, primarily through a much reduced k_h.

E^{2}GFP. E^{2}GFP contains the T203Y mutation (as well as F64L and S65T of "standard" eGFP) and therefore shows the

dx.doi.org/10.1021/bi3016839 | Biochemistry 2013, 52, 2482−2491

Scheme 2

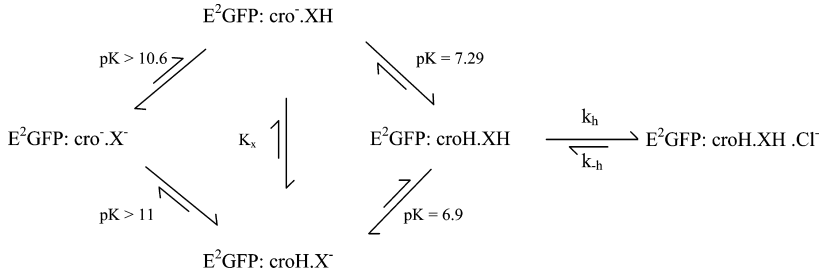

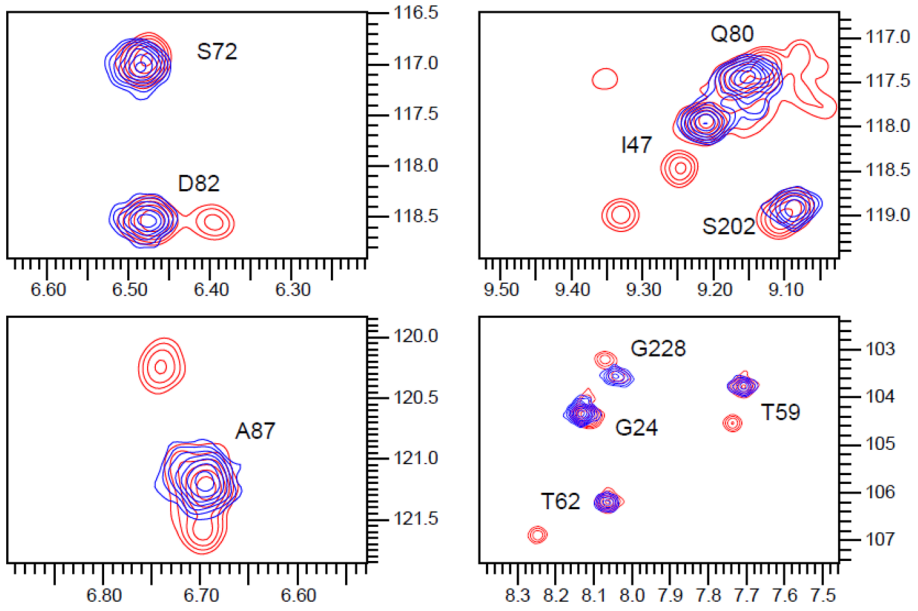

Figure 4. Sections of $^{1}H-^{15}N$ HSQC spectra of mYFP 10C in the absence (blue) and presence of 10 mM fluoride (red). Among residues that change very little (S72 and S202), some residues double (D82, T59, and T62) while others appear in at least three peaks such as A87 and I47. The abscissa shows ^{1}H in parts per million and the ordinate ^{15}N in parts per million.

red-shifted emission characteristic of the YFP family. Initial interest in this mutation arose from its photoswitching behavior,[25] but later studies showed the fluorescence emission was sensitive to chloride, with a K_d of 12 mM for the protonated state.[13] As found with wild-type GFP, E^2GFP shows a significant proportion (~60%) of the protonated chromophore state (A-state) at alkaline pH because of internal proton transfer with a nearby residue X (most likely E222).[22] Scheme 1 therefore needs to be modified to include this internal equilibrium.

Bizzarri et al.[22] determined the microscopic pK values in the absence of halide to be 7.29 and 6.9, which combined to give a macroscopic pK of 6.78 and an internal equilibrium constant K_x for the E^2GFP·croH·X^- ↔ E^2GFP·cro^-·XH reaction of 0.4. Binding of Cl^- to either of these species is assumed to be negligible, because of charge repulsion, as is the concentration of the E^2GFP·cro^-·X^- state, which would exist only at very alkaline pH (>10), beyond which the protein is stable. In our stopped-flow measurements (Figure S4 of the Supporting Information), the instrument was first calibrated to give a 1 V signal for the emission at >530 nm (excitation at 515 nm) at pH 8.0 in the absence of Cl^- where the E^2GFP·croH·XH state is a minor species. The observed signal in pH 6 buffer was 0.22 V, indicating a macroscopic pK of 6.6, comparable with the literature value of 6.78.[22] In the presence of 50 mM NaCl, the observed emission signal at pH 6 was 0.028 V, consistent with an apparent pK of 7.6 (which was confirmed in a separate titration). Such a shift in pK indicates a K_h for binding of Cl^- to the E^2GFP·croH·XH state of ≈5 mM (cf., 12 mM[13]). When the pH was jumped from pH 6 or 8 to a final pH of 6.9 by mixing in the stopped-flow apparatus in the absence of a halide, no transient signals were detected, indicating the proton equilibria were established within the dead time of the instrument, as expected.[22] However, in the presence of 50 mM Cl^-, a transient was observed with a k_{obs} of 0.52 s^{-1} (Figure S4 of the Supporting Information). This value, in conjunction with the equilibrium constant of 5 mM, indicates k_h = 23 M^{-1} s^{-1} and k_{-h} = 0.12 s^{-1}; i.e., both rate constants are an order of magnitude smaller than those for YFP 10C, but the equilibrium constant K_h for Cl^- binding is similar. However, at pH 7, the observed affinity for Cl^- is 20-fold tighter for E^2GFP than for YFP 10C because of the much higher pK of the former.

NMR Spectroscopy of mYFP 10C. Hsu et al.[8] found that Cl^- perturbed the $^{1}H-^{15}N$ HSQC NMR spectra of Venus but concluded the effects were nonspecific because shifts occurred in residues throughout the structure, the shifts were in the fast exchange regime, and similar shifts were induced by NO_3^- anions. Our estimates of the dissociation rate constants for interaction of a specific halide with all YFP variants are in the range of 0.1−1 s^{-1} and should occur in the slow exchange regime. We chose to investigate binding of F^- to YFP 10C, for which specific halide binding had a low K_d, to minimize any

dx.doi.org/10.1021/bi3016839 | *Biochemistry* 2013, 52, 2482−2491

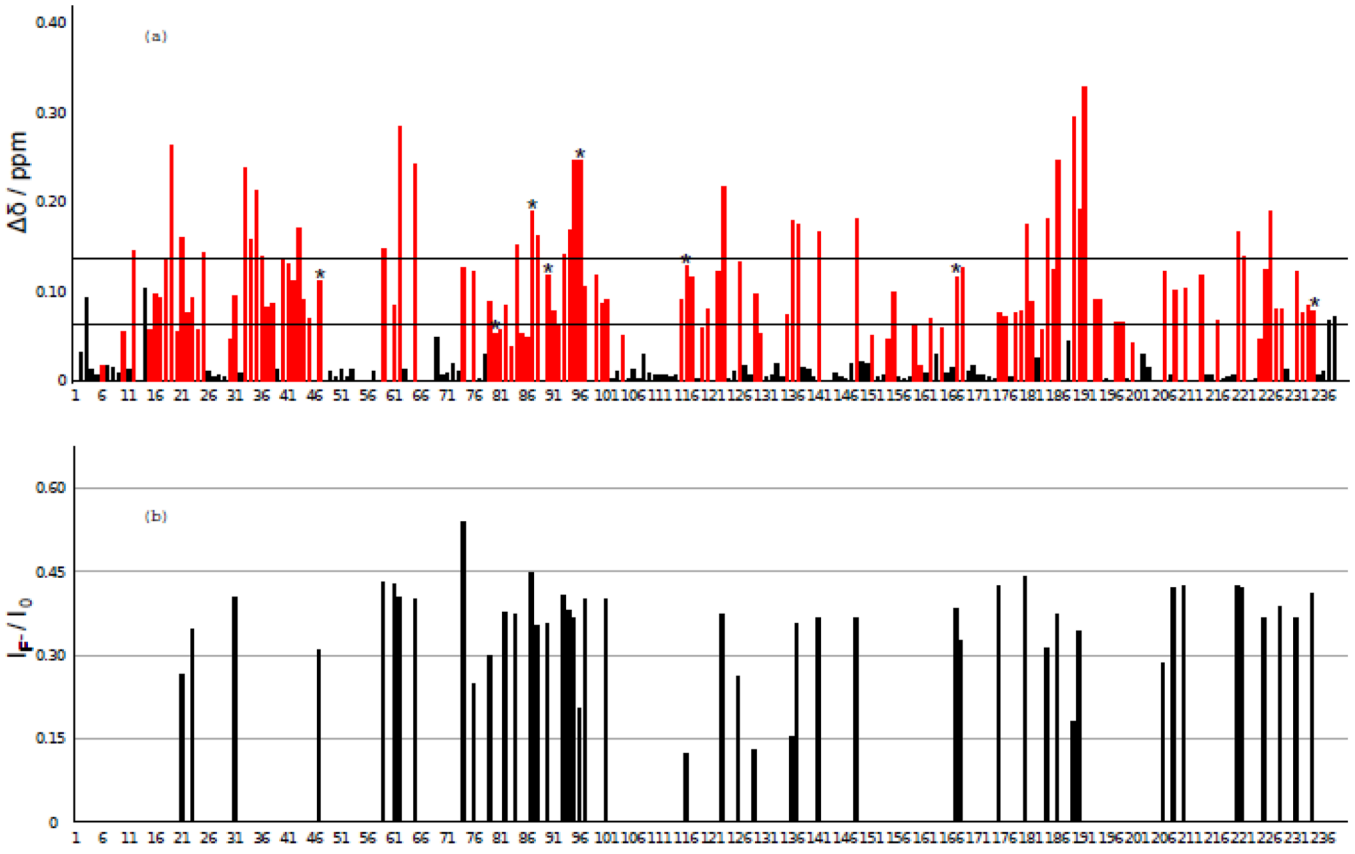

Figure 5. Quantitative analysis of effects of fluoride on the $^{1}H-^{15}N$ HSQC spectrum of mYFP 10C. (a) Combined ^{1}H and ^{15}N chemical shift perturbation plotted against the amino acid sequence. Red bars represent data for amino acids whose peaks double; data for those that do not double are colored black. Amino acids that show more than two peaks in the presence of fluoride are denoted with asterisks. The average chemical shift perturbation and the average perturbation plus one standard deviation are shown as horizontal lines. (b) Relative peak volumes of the fluoride-induced conformer compared to the fluoride-free form calculated for residues for which both peaks were well resolved.

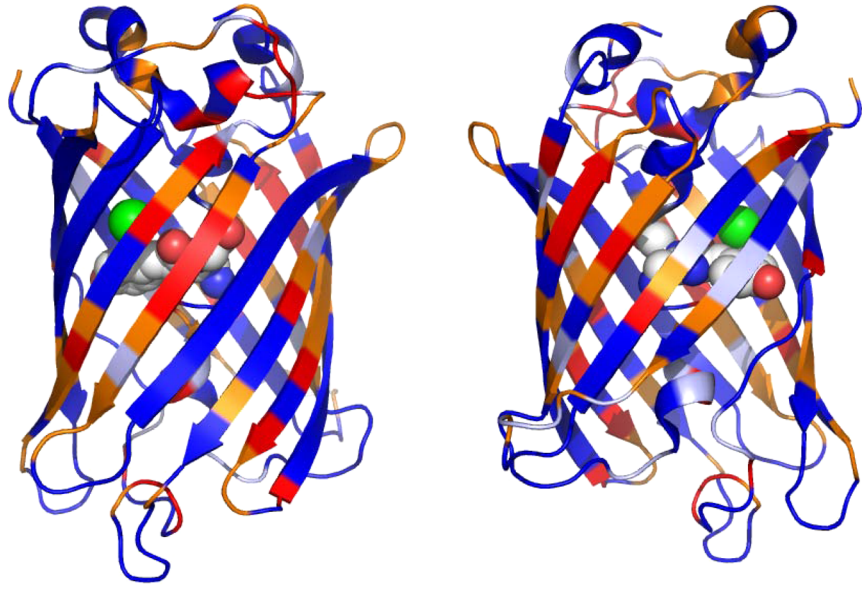

Figure 6. Mapping of the chemical shift perturbations on the crystal structure of YFP. Residues with chemical shift perturbations of more than one standard deviation and smaller than two standard deviations are colored orange, those of more than two standard deviations red, those for which we do not have data light blue, and all others blue. The chromophore is shown in space-filling mode, and the internally bound iodide ion (PDB entry 1f09[12]) is shown as a green sphere. The structure is shown in two orientations related by a 180° rotation around its main axis.

nonspecific effects (apparent K_d at pH 7 of 12 mM). Furthermore, we used the mYFP 10C variant (A206K) to minimize dimerization at the concentrations required for NMR spectroscopy.[26−28] Comparison of ^{15}N HSQC spectra in the

dx.doi.org/10.1021/bi3016839 | *Biochemistry* 2013, 52, 2482−2491

absence and presence of 10 mM NaF showed significant chemical shift perturbations and peak doubling for a substantial number of peaks (Figure 4 and Table S1 of the Supporting Information). Of 210 unambiguously identified residues in the HSQC spectra (from a total of 238 residues in the protein), 108 showed peak multiplication. The affected residues showed no obvious clustering in either the sequence (Figure 5a) or the structure (Figure 6), except for residues close to the chromophore. Integration of peak volumes for residues where signals for the F−bound and apo bound forms were well-resolved showed a ratio of around 0.35 ± 0.09 across the length of the protein (Figure 5b). This corresponds to an apparent K_d at pH 7 of 18 mM (range of 12−27 mM based on the standard deviation), which is comparable to the value of 12 mM determined from the stopped-flow data given above. In a few cases, there were clearly more than two peaks in the presence of F^-, suggesting the existence of multiple states.

DISCUSSION

Previous studies have established a tight coupling between binding of a halide and a proton to YFP variants, i.e., those constructs containing a T203Y mutation.[3,9,12,13] A general scheme for describing the equilibrium is shown in Scheme 3.

Scheme 3

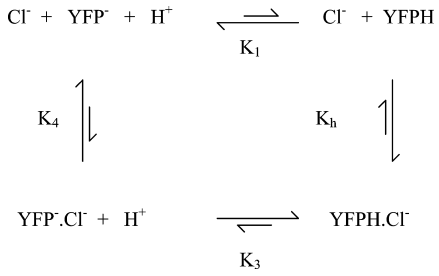

$YFP^-\cdot Cl^-$ is a very unstable state with a K_4 of ≥200 mM for YFP 10C, while the $YFPH\cdot Cl^-$ state has a K_2 value of ∼5 mM[12] (cf. 3.2 mM from our data) for Cl^- dissociation. As a result of this thermodynamic linkage, Cl^- binds weakly to YFP at high pH values and the apparent pK of the YFP chromophore is shifted to a higher pK value with an increasing Cl^- concentration $\{pK_{app} = pK + \log[[Cl^-]/([Cl^-] + K_2)]\}$. Indeed, the value of K_4 is sufficiently weak that it cannot be determined with certainty. Wachter et al.[12] estimate a K_4 value of 288 mM from their fitting procedure (their Table 3), but they also report an apparent dissociation constant for Cl^- at pH 8 of 2160 mM (their Table 1), which should be a lower limit for K_4. Given the difficulty of correcting for nonspecific effects of ionic strength (e.g., on buffer pK values) when halide concentrations are >200 mM, this value is best considered a lower limit for K_4. Arosio et al.[13] report comparable findings for binding of Cl^- to E^2GFP with a fitted estimate for K_4 of 2.5×10^{44} mM; i.e., the $YFP^-\cdot Cl^-$ state makes no contribution to the scheme, and not surprisingly, they report that an equally good fit is obtained when this species was ignored (thus confirming there is no information in the data that can provide a unique value for K_4). In addition, the kinetics of the pathway via K_3 and K_4 lead to a different dependence of k_{obs} on Cl^- concentration and H^+ concentration (see the Supporting Information) and are not compatible with our experimental data (Figure 1). Thus, Scheme 3 is effectively reduced to the Scheme 1 used in our analysis.

Compared to extensive equilibrium binding studies, there have been few studies of the kinetics of binding of a halide to YFP variants. Jayaraman et al.[9] presented stopped-flow records for binding of Cl^- to the YFP-H148Q variant that showed responses on the millisecond to second time scale, but their derived rate constants are untenable. Galietta et al.[10] reported observed rate constants in the range of 0.47−18 s^{-1} for binding of Cl^- to a variety of YFP-H148Q mutants, under conditions where the transient was dominated by the contribution of k_{-h}. Arosio et al.[13] commented that equilibrium for binding of a halide ion to E^2GFP was reached within a few seconds, but they did not conduct detailed kinetic studies. Here we extend our studies on YFP 10C[16] and show that the slow protonation reaction, which we previously reported, is coupled to halide binding. Table 2 summarizes our kinetic and derived equilibrium data when analyzed using a two-step mechanism (Scheme 1) for halide binding. In general, F^- binds more tighly than Cl^-, but this can arise from an increased association rate constant or a reduced dissociation rate constant. On the other hand, YFP variants selected for weak halide binding show reduced levels of binding primarily through a markedly reduced association rate constant. All values for k_h are more than 10^7 times slower than that of a diffusion-controlled reaction, suggesting halides bind internally to YFP during a rare "breathing" event that opens the entrance to the binding site. This is consistent with structural data that show the sites occupied by a halide are essentially buried[12,13] and halide ions cannot access from the solvent without a transient opening of an entrance tunnel. Furthermore, Wachter et al.[12] considered that the cavity sizes of YFP apo states are too small to accommodate halide ions, even for high-affinity variants, and therefore, the cavity must remain slightly expanded once a halide has entered during a breathing event. This could be the reason why the conformational change that occurs during halide binding appears to be propagated throughout the structure (Figure 6).

While halide affinity has been rationalized in terms of some specific interactions with amino acid side chains, it is likely that the breathing motions that control the kinetics arise from multiple interactions and are more difficult to pinpoint. YFP variants share the common T203Y substitution, which red-shifts the absorption and emission compared with those of GFP. The tyrosine hydroxyl is within bonding distance of the halide and contributes to the potential of all the YFP proteins studied here to bind halide.[12] R96 is also close to the internal halide atom and would contribute to charge stabilization of a bound anion.[12] However, crystal structures of other YFP variants have been recently documented where halides bind internally but up to 10 Å from 203Y (e.g., http://dx.doi.org/10.2210/pdb3ssh/pdb). The Q69M substitution of Citrine has a large effect by blocking access to the halide binding cavity (the k_h for Cl^- is reduced 40-fold and that for F^- reduced 1800-fold, cf., YFP 10C), but it has little (<3-fold) effect on the dissociation rate constants. The larger effect of this substitution on the association reaction of F^- (hydrated radius of 3.52 Å) compared with that of Cl^- (hydrated radius of 2.5 Å) suggests that the kinetics of dehydration of the halide anion also influence the association reaction. The results for mVenus are more difficult to rationalize in terms of individual substitutions. Comparison with sYFP shows that the V68L substitution contributes to weakening of halide affinity by ∼4-fold, although it is 8 Å from the ion itself. A similar decrease in affinity attributed to V68L was reported for YFP 10C compared with

dx.doi.org/10.1021/bi3016839 | Biochemistry 2013, 52, 2482−2491

its revertant.[12] The F64L mutation is 12 Å away and was proposed to reduce the level of binding of a halide via Venus dimerization, which could block access of the halide to the entrance tunnel.[6] However, we also see a large decrease in the affinity of the halide for mVenus compared with mYFP 10C, in which the A206K mutation reduces the level of dimerization.[19,20,29] Furthermore, E^{2}GFP also contains the F64L mutation, yet this retains high Cl^- affinity. We suggest that the combined mutations of Venus control the relative motions of the backbone, which, in turn, control the breathing motion.

Hsu et al.[8] concluded that Venus bound Cl^- nonspecifically on the basis that a comparable fluorescence quench was induced by NO_3^- and perturbations to the NMR spectra were observed in residues distributed throughout the protein, particularly the loop regions. However, the halide binding cavity is large enough to accommodate NO_3^- ions,[9,12] and therefore, the first observation does not provide rigorous support for the perturbations being due to nonspecific binding to surface residues. In the case of binding of F^- to mYFP 10C, we also found that perturbations in the ^1H and ^{15}N chemical shifts occurred in residues distributed throughout the protein, although in this case F^- binding appears to be predominantly to an internal site based on the kinetics (Figures 4 and 5). Peaks became split on partial saturation with F^-, indicative of the slow exchange regime. The peak shifts observed by Hsu et al.[8] with Venus were indicative of fast exchange, and hence, the perturbations they report at 400 mM NaCl are probably dominated by nonspecific surface interactions of Cl^-.

The chemical shift difference of the YFP 10C species in the presence of F^- can be used to calculate an upper limit for the exchange rate. In the plot of the combined chemical shift perturbations (Figure 5a), with the exception of the termini, the transition of single peaks to doublets is around 0.06 ppm and corresponds to 40 Hz, which can be taken as the upper limit of the exchange rate creating two separate peaks for the exchanging species. Assuming distinct peaks arise from processes more than an order of magnitude slower, we conclude the exchange rate constant is $<4\ s^{-1}$. This value is compatible with but distant from the stopped-flow results, where $k_{obs} = k_{happ}[F^-] + k_{-h} = 0.13\ s^{-1}$ at ~35% saturation of the F^- binding site. However, our unsuccessful efforts to obtain exchange cross-peaks[30] with a mixing time of 100 ms suggest that the exchange rate obtained from the chemical shift perturbations is a very conservative estimate. Examples from the literature show that using comparable mixing times, exchange cross-peaks can be obtained down to values of $1\ s^{-1}$.[31]

Our NMR results have some similarities to those of Seifert et al.,[26] who measured $^1H-^{15}N$ HSQC spectra of GFPuv (F99S/M153T/V163A) and the GFPuv H148G variant. They found peak splitting for residues throughout the structure indicative of slow exchange for the latter construct, in a buffer comprising 115 mM NaCl and 20 mM phosphate. Although GFP variants generally bind halides much more weakly than YFP variants, mutation of H148 promotes access of halides to YFP constructs.[9−11] It is therefore possible that the two conformations of GFPuv (H148G) identified by Seifert et al.[26] represent the Cl^--bound and Cl^--free states. The β-barrel structure of GFP is thought to provide a stable framework that is rigid on the picosecond to nanosecond time scale.[26] The rigidity of the β-barrel may therefore force the whole protein to take on a small but global rearrangement in response to halide binding, rather than a larger but local change close to the halide binding site. Another possible explanation of multiple split peaks and perturbations throughout the structure may come from multiple internal halide binding sites. The pdb coordinates for several YFP mutants (3sso, 3ssp, 3sst, 3ssv, 3ssy, 3sve, 3sry, 3ssh, 3ssk, 3ssl, 3sto, 3sv5, 3svb, 3svc, and 3svd), although they are yet to be fully documented, show a range of internal halide binding sites, located both above and below the chromophore, but still within 7 Å of the chromophore imidazolinone oxygen atom and close to β-strands 4, 8, and 9. Interestingly, the general region of halide binding correlates with a clustering of large chemical shift perturbations in residues in β-strands 4 and 9, while residues in more distant β-strands, including those on the opposite face (strands 1−3), could be perturbed via a movement in the chromophore, whose aromatic character could translate small positional changes into large chemical shifts of neighboring residues.[32]

In terms of practical applications of YFP in cell biology (e.g., as a FRET acceptor), we confirm that Citrine and Venus bind Cl^- with such a weak affinity as to be unaffected by Cl^- under most physiological conditions. sYFP is less satisfactory in this regard. However, all these variants bind Cl^- with sufficient affinity that protein folding studies using molar concentrations of guanidinium hydrochloride could be compromised (cf. ref 8). In single-molecule assays, all these preparations have the capacity to blink on a time scale of seconds in halide-containing buffers, because of reversible halide binding. Such events would be less frequent for Citrine and Venus than for YFP 10C, but the dark states should still be detectable with mean lifetimes ($1/k_{-h}$) in the range of 0.5−12 s.

■ ASSOCIATED CONTENT

Supporting Information

Relationship to previous work, derivation of kinetic equations, and pK values of Venus (Figures S1−S3, respectively), stopped-flow records for binding of a halide to or dissociation of a halide from YFP 10C, mYFP 10C, sYFP, and E^{2}GFP, and F^--induced HSQC shifts for mYFP 10C (Table S1). This material is available free of charge via the Internet at http://pubs.acs.org.

■ AUTHOR INFORMATION

Corresponding Author

*Present address: Department of Chemistry and Biochemistry, University of California, Santa Cruz, CA 95064. Phone: (831) 469-1380. Fax: (831) 469-2935. E-mail: cbagshaw@ucsc.edu.

Present Address

†Cardiovascular & Randall Division, King's College London, London SE1 1UL, U.K.

Author Contributions

H.E.S., R.D., and J.B. prepared materials and performed fluorescence measurements. F.W.M. and M.P. performed and analyzed NMR data. C.R.B. analyzed the kinetic data and wrote the paper with input from all authors.

Funding

This research was supported by The Leverhulme Trust.

Notes

The authors declare no competing financial interest.

■ ACKNOWLEDGMENTS

We thank Nina Bhanji for assistance in preparation of some of the fluorescent proteins and Jagadeesh Radru Raja for preliminary studies of sYFP. We thank Dr. Dorus Gadella for the sYFP clone.

■ ABBREVIATIONS

cro, chromphore formed from residues 65−67; GFP, green fluorescent protein; HSQC, heteronuclear single-quantum coherence; YFP, yellow fluorescent protein (mYFP, monomeric YFP; sYFP, super YFP).

■ REFERENCES

(1) Tsien, R. Y. (1998) The green fluorescent protein. *Annu. Rev. Biochem. 67*, 509−544.

(2) Seward, H. E., and Bagshaw, C. R. (2009) The photochemistry of fluorescent proteins: Implications for their biological applications. *Chem. Soc. Rev. 38*, 2842−2851.

(3) Wachter, R. M., and Remington, S. J. (1999) Sensitivity of the yellow variant of green fluorescent protein to halides and nitrate. *Curr. Biol. 9*, R628−R629.

(4) Griesbeck, O., Baird, G. S., Campbell, R. E., Zacharias, D. A., and Tsien, R. Y. (2001) Reducing the Environmental Sensitivity of Yellow Fluorescent Protein. *J. Biol. Chem. 276*, 29188−29194.

(5) Nagai, T., Ibata, K., Park, E. S., Kubota, M., Mikoshiba, K., and Miyawaki, A. (2002) A variant of yellow fluorescent protein with fast and efficient maturation for cell-biological applications. *Nat. Biotechnol. 20*, 87−90.

(6) Rekas, A., Alattia, J. R., Nagai, T., Miyawaki, A., and Ikura, M. (2002) Crystal structure of Venus, a yellow fluorescent protein with improved maturation and reduced environmental sensitivity. *J. Biol. Chem. 277*, 50573−50578.

(7) Salonikidis, P. S., Niebert, M., Ullrich, T., Bao, G., Zeug, A., and Richter, D. W. (2011) An ion-insensitive cAMP biosensor for long term quantitative ratiometric fluorescence resonance energy transfer (FRET) measurements under variable physiological conditions. *J. Biol. Chem. 286*, 23419−23431.

(8) Hsu, S. T., Blaser, G., Behrens, C., Cabrita, L. D., Dobson, C. M., and Jackson, S. E. (2010) Folding study of Venus reveals a strong ion dependence of its yellow fluorescence under mildly acidic conditions. *J. Biol. Chem. 285*, 4859−4869.

(9) Jayaraman, S., Haggie, P., Wachter, R. M., Remington, S. J., and Verkman, A. S. (2000) Mechanism and cellular applications of a green fluorescent protein-based halide sensor. *J. Biol. Chem. 275*, 6047−6050.

(10) Galietta, L. J., Haggie, P. M., and Verkman, A. S. (2001) Green fluorescent protein-based halide indicators with improved chloride and iodide affinities. *FEBS Lett. 499*, 220−224.

(11) Markova, O., Mukhtarov, M., Real, E., Jacob, Y., and Bregestovski, P. (2008) Genetically encoded chloride indicator with improved sensitivity. *J. Neurosci. Methods 170*, 67−76.

(12) Wachter, R. M., Yarbrough, D., Kallio, K., and Remington, S. J. (2000) Crystallographic and energetic analysis of binding of selected anions to the yellow variants of green fluorescent protein. *J. Mol. Biol. 301*, 157−171.

(13) Arosio, D., Garau, G., Ricci, F., Marchetti, L., Bizzarri, R., Nifosi, R., and Beltram, F. (2007) Spectroscopic and structural study of proton and halide ion cooperative binding to GFP. *Biophys. J. 93*, 232−244.

(14) Arosio, D., Ricci, F., Marchetti, L., Gualdani, R., Albertazzi, L., and Beltram, F. (2010) Simultaneous intracellular chloride and pH measurements using a GFP-based sensor. *Nat. Methods 7*, 516−518.

(15) Orte, A., Craggs, T. D., White, S. S., Jackson, S. E., and Klenerman, D. (2008) Evidence of an intermediate and parallel pathways in protein unfolding from single-molecule fluorescence. *J. Am. Chem. Soc. 130*, 7898−7907.

(16) McAnaney, T. B., Zeng, W., Doe, C. F., Bhanji, N., Wakelin, S., Pearson, D. S., Abbyad, P., Shi, X., Boxer, S. G., and Bagshaw, C. R. (2005) Protonation, photobleaching, and photoactivation of yellow fluorescent protein (YFP 10C): A unifying mechanism. *Biochemistry 44*, 5510−5524.

(17) Muskett, F. W., Frenkiel, T. A., Feeney, J., Freedman, R. B., Carr, M. D., and Williamson, R. A. (1998) High resolution structure of the N-terminal domain of tissue inhibitor of metalloproteinases-2 and characterization of its interaction site with matrix metalloproteinase-3. *J. Biol. Chem. 273*, 21736−21743.

(18) Williamson, R. A., Carr, M. D., Frenkiel, T. A., Feeney, J., and Freedman, R. B. (1997) Mapping the binding site for matrix metalloproteinase on the N-terminal domain of the tissue inhibitor of metalloproteinases-2 by NMR chemical shift perturbation. *Biochemistry 36*, 13882−13889.

(19) Shi, X., Basran, J., Seward, H. E., Childs, W., Bagshaw, C. R., and Boxer, S. G. (2007) Anomalous Negative Fluorescence Anisotropy in Yellow Fluorescent Protein (YFP 10C): Quantitative Analysis of FRET in YFP Dimers. *Biochemistry 46*, 14403−14417.

(20) Zacharias, D. A., Violin, J. D., Newton, A. C., and Tsien, R. Y. (2002) Partitioning of lipid-modified monomeric GFPs into membrane microdomains of live cells. *Science 296*, 913−916.

(21) Mallik, R., Udgaonkar, J. B., and Krishnamoorthy, G. (2003) Kinetics of proton transfer in a green fluorescent protein: A laser-induced pH jump study. *Proc.—Indian Acad. Sci., Chem. Sci. 115*, 307−317.

(22) Bizzarri, R., Nifosi, R., Abbruzzetti, S., Rocchia, W., Guidi, S., Arosio, D., Garau, G., Campanini, B., Grandi, E., Ricci, F., Viappiani, C., and Beltram, F. (2007) Green fluorescent protein ground states: The influence of a second protonation site near the chromophore. *Biochemistry 46*, 5494−5504.

(23) Kovacs, M., Malnasi-Csizmadia, A., Woolley, R. J., and Bagshaw, C. R. (2002) Analysis of Nucleotide Binding to *Dictyostelium* Myosin II Motor Domains Containing a Single Tryptophan Near the Active Site. *J. Biol. Chem. 277*, 28459−28467.

(24) Kremers, G. J., Goedhart, J., van Munster, E. B., and Gadella, T. W. J. (2006) Cyan and yellow super fluorescent proteins with improved brightness, protein folding, and FRET Forster radius. *Biochemistry 45*, 6570−6580.

(25) Cinelli, R. A. G., Pellegrini, V., Ferrari, A., Faraci, P., Nifosi, R., Tyagi, M., Giacca, M., and Beltram, F. (2001) Green fluorescent proteins as optically controllable elements in bioelectronics. *Appl. Phys. Lett. 79*, 3353−3355.

(26) Seifert, M. H. J., Georgescu, J., Ksiazek, D., Smialowski, P., Rehm, T., Steipe, B., and Holak, T. A. (2003) Backbone dynamics of green fluorescent protein and the effect of histidine 148 substitution. *Biochemistry 42*, 2500−2512.

(27) Georgescu, J., Rehm, T., Wiehler, J., Steipe, B., and Holak, T. A. (2003) Backbone H_N, N, C_α and C_β assignment of the GFPuv mutant. *J. Biomol. NMR 25*, 161−162.

(28) Hsu, S. T., Behrens, C., Cabrita, L. D., and Dobson, C. M. (2009) ^{1}H, ^{15}N and ^{13}C assignments of yellow fluorescent protein (YFP) Venus. *Biomol. NMR Assignments 3*, 67−72.

(29) Nakagawa, C., Nishimura, S., Senda-Murata, K., and Sugimoto, K. (2012) A rapid and simple method of evaluating the dimeric tendency of fluorescent proteins in living cells using a truncated protein of importin α as fusion tag. *Biosci., Biotechnol., Biochem. 76*, 388−390.

(30) Farrow, N. A., Zhang, O., Forman-Kay, J. D., and Kay, L. E. (1994) A heteronuclear correlation experiment for simultaneous determination of ^{15}N longitudinal decay and chemical exchange rates of systems in slow equilibrium. *J. Biomol. NMR 4*, 727−734.

(31) Nooren, I. M., Kaptein, R., Sauer, R. T., and Boelens, R. (1999) The tetramerization domain of the Mnt repressor consists of two right-handed coiled coils. *Nat. Struct. Biol. 6*, 755−759.

(32) Seifert, M. H., Ksiazek, D., Azim, M. K., Smialowski, P., Budisa, N., and Holak, T. A. (2002) Slow exchange in the chromophore of a green fluorescent protein variant. *J. Am. Chem. Soc. 124*, 7932−7942.